Environmental Science & Technology

ARTICLE

pubs.acs.org/est

Simulating the Degree of Oxidation in Atmospheric Organic Particles

Heather Simon*,† and Prakash V. Bhave‡

†Office of Air Quality Planning and Standards and ‡National Exposure Research Laboratory, Atmospheric Modeling and Analysis Division, US EPA, Research Triangle Park, North Carolina 27711, United States

Supporting Information

ABSTRACT: Modeled ratios of organic mass to organic carbon (OM/OC) and oxygen to carbon (n_O/n_C) in organic particulate matter are presented across the US for the first time and evaluated extensively against ambient measurements. The base model configuration systematically underestimates OM/OC ratios during winter and summer months. Model performance is greatly improved by applying source-specific OM/OC ratios to the primary organic aerosol (POA) emissions and incorporating a new parametrization to simulate oxidative aging of POA in the atmosphere. These model improvements enable simulation of urban-scale gradients in OM/OC with values in urban areas as much as 0.4 lower than in the surrounding regions. Modeled OM/OC and n_O/n_C ratios in January range from 1.4 to 2.0 and 0.2 to 0.6, respectively. In July, modeled OM/OC and n_O/n_C ratios range from 1.4 to 2.2 and 0.2 to 0.8, respectively. Improved model performance during winter is attributed entirely to our application of source-specific OM/OC ratios to the inventory. During summer, our treatment of oxidative aging also contributes to improved performance. Advancements described in this paper are codified in the latest public release of the Community Multiscale Air Quality model, CMAQv5.0.

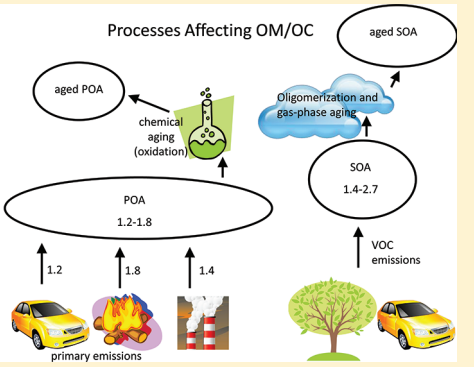

Downloaded via US EPA RESEARCH TRIANGLE PARK on March 12, 2025 at 15:23:56 (UTC).
See https://pubs.acs.org/sharingguidelines for options on how to legitimately share published articles.

1. INTRODUCTION

Many studies have documented a large discrepancy between air quality model results and summertime measurements of particle-phase organic mass (OM).[1−9] Every approach for closing the gap between models and measurements has increased model estimates of secondary organic aerosol (SOA) by raising the stoichimetric yields,[1,10−13] augmenting the list of volatile organic compound precursors that form SOA via gas-phase oxidation,[1,11,13−15] simulating SOA formation in clouds and aqueous droplets,[11,16−19] introducing a new class of SOA precursors [i.e., intermediate volatility organic compounds (IVOCs)] to models,[12,20,21] or parametrizing oxidative aging of OM to reduce its volatility.[1,12,21−26] In the vast majority of modeling studies, results are evaluated against only the total OM or organic carbon (OC) concentrations. Such bulk comparisons are a useful starting point but insufficient for assessing the accuracy of model estimates. A few model evaluation studies have used additional observational constraints such as source-specific tracers of primary organic aerosol (POA);[8,27−29] precursor-specific tracers of SOA;[30,31] isotopic measurements that distinguish fossil-fuel carbon from contemporary carbon;[8,32−34] spectrometric measurements that subdivide OM into hydrocarbon-like, oxygenated, and biomass burning organic factors;[22,30,35,36] and ratios of OM to carbon monoxide.[22]

One very useful constraint that has received little attention in model performance evaluations is the organic mass-to-carbon ratio (OM/OC). This ratio indicates the extent to which OC has been oxidized,[37,38] and that extent is governed by the emission source or gas-phase precursor from which the OC originated[31,39,40] and the subsequent chemical transformations that OC undergoes in the atmosphere (e.g., oxidative aging).[20,41,42] Evaluating OM/OC ratios in models is especially important given that the noncarbon organic mass (NCOM ≡ OM − OC) and OC each make up a substantial portion of fine-particulate mass ($PM_{2.5}$). An accurate representation of OM/OC in models may also improve our estimation of particle properties such as hygroscopicity, volatility, light extinction, and reactivity.

Three major obstacles have prevented the widespread use of OM/OC ratios in model evaluations. First, routine monitoring networks generally measure OC[43−45] and only a few specialized techniques measure OM.[46,47] Thus ambient measurements of the OM/OC ratio are scarce. Second, most models do not calculate the concentrations of both OM and OC, so the modeled OM/OC ratios are unavailable (except in refs 22, 48, 49). Third, the atmospheric processes by which OC is oxidized are poorly understood. They may include heterogeneous reactions of oxidants on particle surfaces,[41,50,51] gas-phase oxidation of semivolatile OC followed by condensation to the particle phase,[21,22,25,26] and condensed-phase reactions involving aqueous chemistry and oligomerization.[18,19,52,53]

Numerous advances in recent years allow us to break through all three obstacles and conduct the first large-scale evaluation of air quality model results against observational estimates of OM/OC. In this study, we refine the US National Emissions Inventory (NEI) and advance the Community Multiscale Air Quality (CMAQ) model to simulate OM/OC ratios across the US during

Received: July 8, 2011
Accepted: November 22, 2011
Revised: November 18, 2011
Published: November 22, 2011

ACS Publications This article not subject to U.S. Copyright. Published 2011 by the American Chemical Society

Table 1. Summary of Measured and Modeled k_{OH} Values for POA Aging

type of study	POCR tracer or surrogate	$k_{OH,eff} \times 10^{11}$ (cm^3 $molec^{-1}$ s^{-1})	relative humidity (%)	reference
laboratory measurements	bis(2-ethylhexyl) sebacate	0.25[a]	30−60	58
	POA tracer compounds	0.04−0.7	75	56
	POA tracer compounds	0.5−3.4	10	57
	POA tracer compounds	0.3−6.2	10	57
	bulk motor oil POA	0.6	10	57
	bulk diesel POA	1.6	10	57
numerical modeling	POCR	0.25	all	this study
	semivolatile and IVOC	0.4−4.0	all	23, 24, 59

[a] Actual rate constant reported as 7.6×10^7 atm^{-1} s^{-1} and converted to cm^3 $molec^{-1}$ s^{-1}, assuming standard temperature and pressure.

a summer and winter month. We evaluate our model results against observational estimates from the Interagency Monitoring of Protected Visual Environments (IMPROVE) ambient network.[54] Advancements discussed in this paper are codified in the newest release of CMAQ, version 5.0 (www.cmaq-model.org).

2. MATERIALS AND METHODS

2.1. Base Model Description (CMAQv4.7.1). The treatment of OM/OC ratios in primary $PM_{2.5}$ is grossly simplified in most photochemical models. For example, in versions of CMAQ that precede version 5.0, total POA mass is not explicitly modeled. Instead, primary organic carbon (POC) is emitted and transported while the remaining noncarbon portion of POA is lumped with other unspeciated material.[3] As a result of this lumping, earlier versions of the CMAQ model could not simulate variations in the OM/OC ratio of POA from different source types. Furthermore, the effect of oxidative aging on OM/OC was approximated crudely during the postprocessing of CMAQ results (see eq 2 of ref 55). POA in CMAQ is treated as nonvolatile. The SOA treatment in CMAQ is explained elsewhere,[1] so only a brief description is provided here. CMAQv4.7.1, which is the base version used in this study, allows three biogenic and four anthropogenic VOC classes to form a variety of semivolatile and nonvolatile products after reacting with gas-phase oxidants. In addition, nonvolatile SOA can be formed via aqueous-phase oxidation of glyoxal and methylglyoxal or oligomerization of semivolatile SOA. In total, 19 separate SOA types are formed and tracked. The OM/OC ratio of each SOA species is given in Table 1 of ref 1, from which the modeled concentrations of SOA can be disaggregated easily into OC and NCOM. Throughout this study, the treatment of SOA is identical to that described in ref 1.

2.2. Revised Emissions Sensitivity. In this study, a modified version of CMAQv4.7.1 is created to allow the explicit tracking of any NCOM associated with POC (PNCOM). In our first sensitivity run, hereafter referred to as the "revised emissions simulation", PNCOM emissions are computed according to source type (0.25 × POC from mobile sources, 0.7 × POC from all sources of biomass burning, and 0.4 × POC from all other sources). These coefficients are obtained from a literature review described in section S3.7.3 of ref 40. Physical processes, such as transport, coagulation, and deposition are applied identically to PNCOM and POC.

2.3. Simulation of POA Aging. A second sensitivity scenario, the "POA aging simulation", includes both the revised emissions treatment described above and a parametrization to simulate oxidative aging of POA in the atmosphere. We simulate POA aging as a second-order heterogeneous reaction between reduced primary organic carbon (POCR) and gas-phase hydroxyl radicals, producing PNCOM as shown in reaction 1. Note that PNCOM is attached to the primary carbon but itself can be either primary or secondary in nature.

$$\mathrm{POCR} + \mathrm{OH} \xrightarrow{k_{OH,eff}} \mathrm{POCO} + \mathrm{OH} + \mathrm{PNCOM} \quad \text{(reaction1)}$$

In reaction 1, POCO represents oxidized POC, and $k_{OH,eff}$ is an effective rate constant described below. By design, POA that is already highly oxidized (e.g., POA emitted from forest fires) ages at a slower rate than POA that is reduced (e.g., diesel exhaust). Note that OH is not consumed by reaction 1. This is consistent with previous updates to CMAQ, in which we purposefully prohibited reactions with highly uncertain emissions and/or reaction rates (e.g., sesquiterpenes) from consuming oxidants so that the least certain aspects of aerosol chemistry would not affect CMAQ predictions of ozone.[1] With reaction 1 we intended to approximate the net result of a multistep process that is the subject of ongoing investigation. The steps are not fully understood, but they likely include volatilization of POA, gas-phase and heterogeneous oxidation, deposition of some gas-phase material and its oxidation products to the surface, and recondensation of the low vapor-pressure products that remain airborne.[20]

Actual and effective rate constants have been measured for various POA tracer compounds,[56,57] a POA surrogate compound,[58] and for bulk POA[57] (Table 1). The rate constants span a very wide range [$(0.04-6.2) \times 10^{-11}$ cm^3 $molec^{-1}$ s^{-1}], which can be substantially narrowed by only considering tests conducted above 20% relative humidity, because the drier conditions are of limited relevance in photochemical modeling applications. From this narrower range of values [$(0.04-0.7) \times 10^{-11}$], we choose for CMAQ an intermediate $k_{OH,eff} = 0.25 \times 10^{-11}$. We found no experimental data to warrant a temperature or pressure dependence of $k_{OH,eff}$. As seen in Table 1, the $k_{OH,eff}$ value selected here is slower than k_{OH} rates applied when aging gas-phase organic compounds in the volatility basis set (VBS) framework of other models: $(0.4-4) \times 10^{-11}$.[12,22,25,26,36,49,59] This is discussed in section 4.

For implementation of reaction 1 in CMAQ, we define moles of POCR (n_{POCR}) by subtracting the moles of oxygen in PNCOM (n_{PNCOM_O}) from the moles of POC (n_{POC}).

$$n_{POCR} \equiv n_{POC} - n_{PNCOM_O} \quad (1)$$

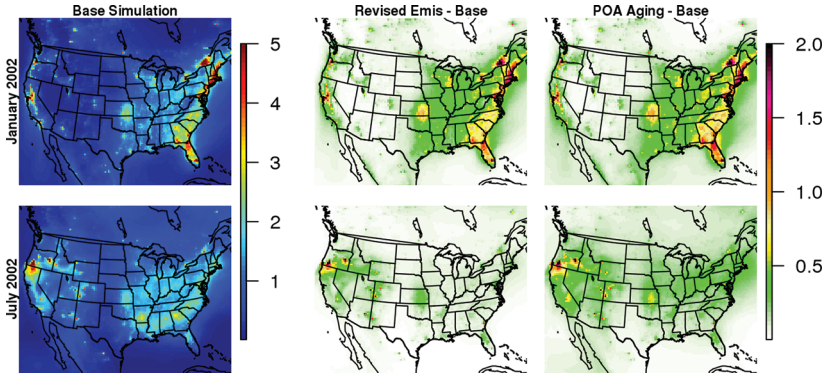

Figure 1. (Left) Monthly average OM concentrations ($\mu g/m^3$) from the base simulation using CMAQv4.7.1. (Middle) The increase in modeled OM concentrations that result from our emission inventory revisions. (Right) The net OM increase from revising the POA emissions and including reaction 1.

In the remainder of this paper, variables in the form of n_X are in molar units and all other variables (e.g., OM, OC, NCOM, POA) represent mass concentrations. To apply eq 1 and incorporate reaction 1 into CMAQ, we need to make some assumptions for calculating n_{PNCOM_O}. First, we assume that NCOM is comprised entirely of oxygen and hydrogen.

$$OM = n_H + 16n_O + 12n_C \quad (2)$$

This assumption ignores the NCOM contributions from nitrogen, sulfur, and other heteroatoms, but that is expected to have negligible impact on our results. Average ratios of n_N/n_C in ambient OM are less than 0.02[46] and other elements also contribute small fractions to OM.[60,61]

Second, we assume a linear relationship between the hydrogen-to-carbon ratio (n_H/n_C) and the oxygen-to-carbon ratio (n_O/n_C) within POA.

$$\frac{n_O}{n_C} + \frac{n_H}{n_C} = 2 \quad (3)$$

Heald et al.[37] derived this empirical relationship from laboratory and field measurements of various OM types, including POA, SOA, and total ambient OM at near-source and remote locations. Note that the limits of eq 3 can be interpreted physically. When $n_O/n_C = 0$ and $n_H/n_C = 2$, the OM is composed of very large alkanes. The other extreme ($n_H/n_C = 0$ and $n_O/n_C = 2$) places all carbon in large esterified polyketones or carbon dioxide.

Combining eqs 2 and 3 yields a relationship between NCOM and n_O,

$$n_O = \frac{NCOM}{16 + \frac{n_H}{n_O}} \quad (4a)$$

In which

$$\frac{n_H}{n_O} = \frac{\frac{44}{12} - \frac{OM}{OC}}{\frac{OM}{OC} - \frac{14}{12}} \quad (4b)$$

These equations are derived in the Supporting Information.

In CMAQ, we apply eq 4 only to POA and set limits on n_{PNCOM_O} to avoid a negative value of n_H/n_O.

$$n_{PNCOM_O} = \begin{cases} 0 & \text{if } \frac{POA}{POC} \le \frac{14}{12} \\ \frac{PNCOM}{16 + \frac{n_{PNCOM_H}}{n_{PNCOM_O}}} & \text{if } \frac{14}{12} < \frac{POA}{POC} < \frac{44}{12} \\ \frac{PNCOM}{16} & \text{if } \frac{44}{12} \le \frac{POA}{POC} \end{cases} \quad (5a)$$

$$\frac{n_{PNCOM_H}}{n_{PNCOM_O}} = \frac{\frac{44}{12} - \frac{POA}{POC}}{\frac{POA}{POC} - \frac{14}{12}} \quad (5b)$$

Recent work suggests that laboratory SOA may follow a shallower slope than the line defined by eq 3.[62] When coupled with the fact that eq 3 was derived from all types of OM, it is conceivable that POA follows a steeper slope, but that is currently too speculative to parametrize in CMAQ. In practice, POA/POC will remain much smaller than 44/12 in CMAQ because reaction 1 stops when $n_{PNCOM_O}/n_{POC} = 1$ (see eq 1).

A physiochemical interpretation of eq 3 is that every two oxidation reactions, on average, result in the conversion of a methyl group ($-CH_3$) into a carboxylic acid group ($-COOH$).[37] Therefore, we assign a molar mass of 15 g/mol to PNCOM formed through aging in CMAQ, representing a loss of one H atom and gain of one O atom with each occurrence of reaction 1. This is modeled as follows:

$$PNCOM_{t+\Delta t} = PNCOM_t + 15n_{POCR}\left(1 - e^{-k_{OH,eff}(OH)\Delta t}\right) \quad (6)$$

2.4. Model Setup. CMAQv4.7.1 and each sensitivity simulation are run for two full-month periods (January and July 2002), each with a 10 day spinup (Dec 22−31, 2001 and Jun 21−30, 2002). Our model domain covers the entire continental US with 36 km square grid cells and 24 vertical layers. Meteorological inputs are created using MM5.[63] Anthropogenic emissions are obtained from the 2002 NEI,[64] which includes a detailed inventory of

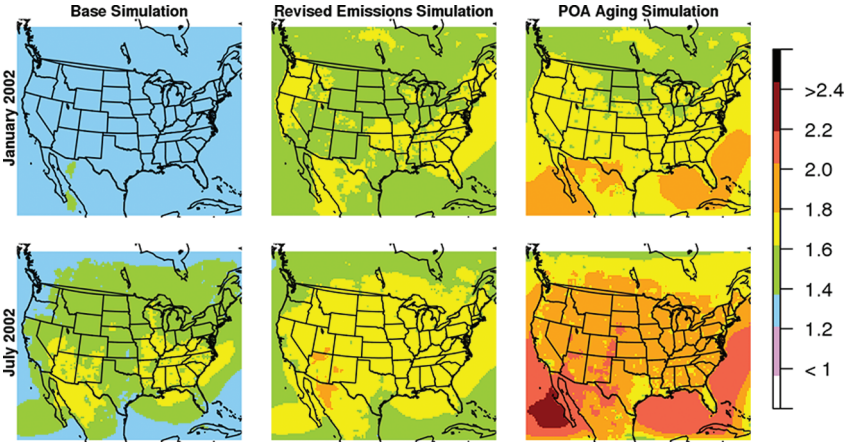

Figure 2. Monthly average OM/OC ratios in the base and sensitivity simulations, calculated as monthly average OM divided by monthly average OC in each grid cell. Note that results shown in the right panel include both revised POA emissions and NCOM formation via reaction 1.

wild fires, and biogenic emissions are estimated using BEIS v3.14.[1] Boundary conditions for all species except PNCOM are extracted from a GEOS-CHEM[65] global simulation of 2002. Boundary concentrations of PNCOM are set uniformly to 0.4 × POC.

3. RESULTS

3.1. Effect on OM and $PM_{2.5}$. Figure 1 displays the increase in modeled OM concentrations after applying source-specific OM/OC ratios to the NEI and POA aging in the CMAQ model. During winter, most of the OM increase is due to our revised emissions rather than POA aging. We find enhancements of over 1.5 $\mu g/m^3$ in many grid cells (see red shading in the upper-middle subplot of Figure 1). These increases are most pronounced in populated areas (e.g., Northeast and Pacific coastal states) due to residential wood burning and in the Southeast due to agricultural and prescribed burning activities in the NEI.[40] During summer, we find substantial OM increases in both sensitivity simulations. Our revised emissions cause 2 $\mu g/m^3$ enhancements in small areas impacted by wildfires, while the POA aging reaction increases OM by 0.5 $\mu g/m^3$ across much broader regions (see the abundance of dark green shading in the lower-right subplot compared to the lower-middle subplot of Figure 1). Although these OM increases will improve the CMAQ underestimates of summertime $PM_{2.5}$ reported previously,[3,55] they will not resolve the documented underestimation of OC because our changes predominantly affect only the NCOM concentrations.

3.2. Gridded OM/OC Ratios. Outputs from all CMAQ simulations are postprocessed to obtain OM/OC ratios in each grid cell. OM is calculated as the sum of POC, PNCOM, and all 19 SOA species. OC is calculated as the sum of POC plus each SOA species divided by its own OM/OC ratio.[1] In the base simulations, PNCOM is approximated as 0.2 × POC, because it is not tracked explicitly in CMAQv4.7.1.

Figure 2 shows monthly average OM/OC ratios across the US during January and July 2002 for the base run and both sensitivity simulations. In both months, the revised emissions increase OM/OC relative to the base simulation, and adding reaction 1 increases those ratios even further. Moreover, the POA aging simulation exhibits a stronger urban-to-rural gradient than the other simulations.

Wintertime OM/OC ratios are dominated by POA, so we see almost no spatial variation in the base run (widespread blue shading in upper-left subplot of Figure 2). Adding source-specific NCOM emissions increases OM/OC to at least 1.4 domainwide. Only in regions where wood smoke is ubiquitous (e.g., the Southeast) do we see lower OM/OC values in urban areas (e.g., Atlanta, Charlotte, Birmingham) than in their rural surroundings due to higher urban concentrations of vehicle exhaust relative to other OM sources. In the winter POA aging simulation, many more urban areas have lower OM/OC ratios than their surroundings (e.g., Los Angeles, Las Vegas, Phoenix, Denver, Dallas, Houston, Atlanta, Miami, Philadelphia). These appear as green dots (OM/OC = 1.4−1.6) in a background of yellow (OM/OC = 1.6−1.8) in the upper-right subplot of Figure 2, reflecting limited aging of POA close to its sources.

The base July simulation exhibits moderate spatial variability in OM/OC due to the changing relative abundance of SOA and POA in different locations. The urban/rural gradient becomes most pronounced in the July simulation with POA aging (see lower-right subplot of Figure 2). For instance, the OM/OC ratio in Los Angeles is about 0.4 less than the surrounding areas versus a 0.2 difference in the base simulation (compare lower-right and lower-left subplots of Figure 2). This sharpened gradient is explained by the time scale of POCR oxidation in reaction 1. Assuming a summer OH concentration of 5 × 10^6 molec/cm^3, POCR has a lifetime of 22 h, which is comparable to the transport of fresh emissions out of an urban area. Turpin and Lim[42] were the first to observe an urban/rural gradient in OM/OC. From ambient measurements in southern California, they deduce an average urban OM/OC ratio of 1.6 and a rural ratio of 2.1. Our July POA aging simulation results in that region match those values closely. One other study of $PM_{2.5}$ in New York has since described urban/rural gradients for OM/OC,[66] and our POA aging simulation results in New York agree well with that study.

The OM/OC values in Figure 2 can be qualitatively compared with a 2-day model simulation of the northeastern US performed by previous investigators.[48] For August 3−4, 2004, they simulated OM/OC ratios between 1.2 and 1.7. Our July simulation with POA aging yields OM/OC ratios between 1.6 and 2.0 across the Northeast. Our results are in better agreement with observations than the low values modeled previously,[48] due to our improved treatment of PNCOM (see section 3.4).

3.3. Gridded n_O/n_C and n_H/n_C Ratios. Although we do not track organic oxygen and hydrogen concentrations in CMAQ, the assumptions made in section 2.3 allow us to convert OM/OC ratios into elemental ratios, n_O/n_C and n_H/n_C, within the modeled

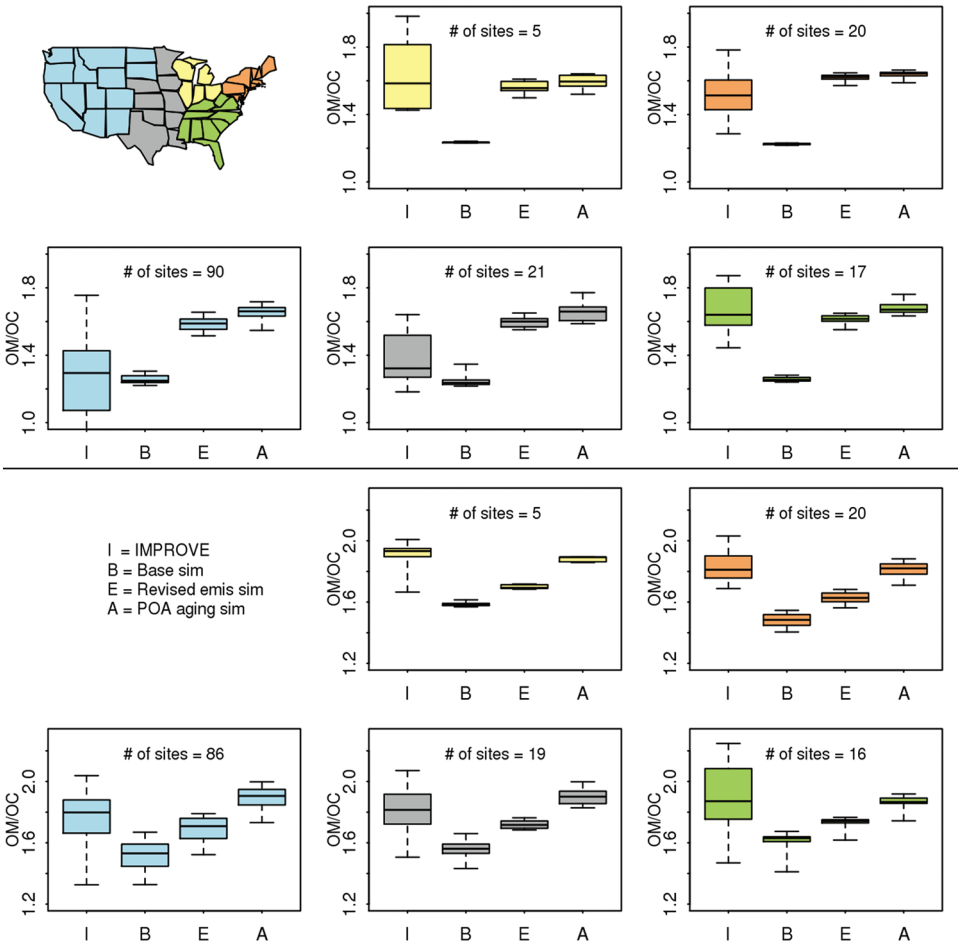

Figure 3. Regional and seasonal evaluation of modeled OM/OC ratios against the observation-based estimates of OM/OC at IMPROVE monitoring sites. Upper plots compare quarter 1 IMPROVE data (January, February, March 2002−2008) with modeled values from January 2002. Lower plots compare quarter 3 IMPROVE data (July, August, September 2002−2008) with modeled values from July 2002. Boxes show the 25th and 75th percentile values among IMPROVE sites within a given region, with whiskers extending to the 5th and 95th percentile values and horizontal lines depicting the median value in the given region.

OM (see Supporting Information). Figure S1 (Supporting Information) displays these ratios from all three simulations for both months. Our modeled ratios can be compared against the growing body of ambient data collected by high resolution time-of-flight mass spectrometry (see Table S1, Supporting Information). Although the currently available data are rather sparse (all collected after 2005 and much of them outside our study domain[46,67,68]), they are useful for testing some of our model results. As summarized in Table S1 (Supporting Information), all measurements of POA and laboratory SOA have n_O/n_C ratios less than 0.5, whereas ambient OM measurements fall between 0.3 and 0.7 in freshly emitted plumes and between 0.6 and 1.1 in aged air masses. CMAQ results are in reasonable agreement with these data (lower-right subplots of Figure S1, Supporting Information). The POA aging scenario yields n_O/n_C ratios between 0.3 and 0.5 in January and between 0.4 and 0.8 in July, with slightly lower values in large urban areas. Modeled n_O/n_C ratios in central California (0.5−0.6) generally agree with measurements in that region.[69] Model estimates in the Pacific Northwest (0.4−0.7) are slightly lower than average measured values.[69,70] From these limited comparisons, the POA aging scenario gives more realistic n_O/n_C estimates than the base simulation. Future wintertime measurement campaigns should test the latitudinal n_O/n_C gradients that are quite pronounced in our model results (see Figure S1, Supporting Information). It is noteworthy that n_O/n_C ratios modeled in Greece by others[49] lie between 0.4 and 0.7, which is in the same range as our July POA aging simulation. Model estimates over Mexico City[22] range from 0.2 to 0.3 or 0.5 to 0.6, depending on which assumptions are made in the VBS framework to simulate IVOC aging. The higher ratios from that study are in agreement with our July POA aging simulation.

Ambient measurements of n_H/n_C are not readily available, but our January and July revised emissions sensitivity simulations are in agreement with measurements of laboratory POA and SOA (n_H/n_C = 1.45−1.9).[46,71,72] As expected, the POA aging scenario yields lower n_H/n_C values than the base and revised emissions scenarios.

3.4. Comparison of Modeled OM/OC with Observation Based Estimates. The model evaluations above provide limited insight because the measurements of OM/OC, n_O/n_C, and n_H/n_C are so sparse. However, a few recent studies have estimated OM/OC ratios from ambient measurements at ∼100 IMPROVE sites across the US.[54,73,74] Of those studies, only one provides season-specific OM/OC ratios,[54] which are most valuable for evaluating our CMAQ model results. In that study, the investigators pooled 7 years of IMPROVE data (2002−2008)

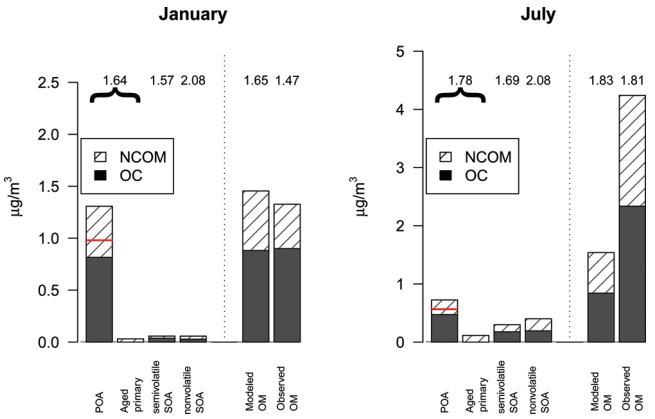

Figure 4. Comparison of OM constituents in the POA aging scenario to ambient data averaged over all IMPROVE monitoring sites for January (left) and July (right). The number above each bar represents the OM/OC ratio for that OM constituent. The red line on the POA bar shows the NCOM concentration from the base simulation.

by quarter and applied sophisticated statistical analyses to estimate quarter-specific OM/OC ratios at each site. We compare January model results (shown in Figure 2) against the IMPROVE data from quarter 1 and our July model results against the quarter 3 IMPROVE data.

Model evaluation results are displayed in Figure 3. Due to uncertainties in the statistical method used to estimate OM/OC ratios from the ambient measurements (e.g., incomplete characterization of measurement uncertainty, multicolinearity, and within-season variability),[54] we do not conduct the evaluation at each monitoring site individually, but instead pool the data into five US regions and look for overlapping interquartile ranges as the indicator of good model performance. Figure 3 shows that the base model configuration (CMAQv4.7.1) systematically underestimates the IMPROVE data, except in the Western region during winter. Adding NCOM emissions and reaction 1 in CMAQ brings the modeled OM/OC ratios into much better agreement with the IMPROVE data (compare box plots "I" and "A" in Figure 3). The summertime model evaluations show this most clearly (lower half of Figure 3). At the 20 northeastern sites, for example, the IMPROVE data suggest a median summertime OM/OC ratio of 1.81, whereas the base model yields only 1.48 and the POA aging scenario gives a ratio of 1.82. A similar improvement in model performance is found across the other regions during summer. In the wintertime, our treatment of NCOM emissions yields substantial improvements in model performance in the Great Lakes, Northeast, and Southeast regions (compare box plots "I" and "E" in the upper-right panels of Figure 3). The only instances where our model enhancements seem to degrade model performance are in the Western and Central regions during winter. The unusually low OM/OC ratios obtained from the IMPROVE data in those regions (1.29 and 1.32) may be due to uncertainties in the statistical method.[54] Previous measurement studies have found higher values in Texas and Arizona (1.6) on an annual average[74] and Southern California (1.8−3.0) during winter months.[42]

The IMPROVE data generally exhibit more within-region variability than the modeled OM/OC ratios (compare height of each box in Figure 3). Only part of this large spread in the IMPROVE data can be attributed to uncertainty inherent in the statistical method (standard error in OM/OC = ±0.1).[54] Given that the IMPROVE monitors are mostly located in national parks and wilderness areas, which are typically representative of regions much larger than a model grid cell, we conclude that our model results systematically underestimate the spatial variability in rural OM/OC ratios.

4. DISCUSSION

Results from our POA aging simulation are noticeably improved over the base CMAQ configuration, when compared against OM/OC and n_O/n_C ratios from ambient measurements. One unanswered question is, "How do the new model results compare against observations of total OM and OC?" Figure 4 shows excellent agreement in January. The average modeled OM concentration across all IMPROVE sites is 1.45 $\mu g/m^3$ (OC = 0.88 and NCOM = 0.57 $\mu g/m^3$), and the IMPROVE OM during quarter 1 averages to 1.32 $\mu g/m^3$ (OC = 0.90 and NCOM = 0.42). Figure 4 also shows that the wintertime modeled OM is almost entirely primary, with SOA and PNCOM from reaction 1 contributing only 0.12 and 0.03 $\mu g/m^3$, respectively. Without our model enhancements, the total OC agrees well with observations, but NCOM is underestimated by a factor of 2 (see the red line in the left panel of Figure 4). The July results show a very different picture (right panel of Figure 4). Although the modeled OM/OC ratio (1.83) matches very well with the IMPROVE data (1.81), the modeled OC and NCOM concentrations fall 1.50 and 1.20 $\mu g/m^3$ short of the IMPROVE data, respectively (compare bars on the right side of the right panel in Figure 4). This highlights a major error in photochemical models that persists in spite of our model enhancements. Closing the gap between modeled and measured OC will require an additional 2.70 $\mu g/m^3$ of OM with an average OM/OC of 1.8. In addition, this would likely mean that PNCOM will have substantially less influence on the total OM/OC ratio than demonstrated by these simulations.

Throughout this study, we model POA as nonvolatile. Recent work suggests that POA is semivolatile and that oxidation of POA vapors proceeds substantially faster than the heterogeneous process modeled here.[21] However, Figure 4 suggests that reaction 1 adequately captures the net effect of POA volatilization, rapid oxidation of vapors, and recondensation during the winter season. On the basis of Figures 3 and 4, it is not obvious that a more explicit treatment of these steps would improve model performance during summer. For example, volatilization of POA would lead to further underestimation of OC and OM near sources. A faster gas-phase oxidation rate might cause overestimation of the OM/OC ratio. While it is possible that the OC and NCOM shortfalls in July are explained by large sources of IVOCs, which are missing from the NEI, testing of that hypothesis awaits (1) accurate quantification of IVOC emissions, (2) incorporation of the revised emissions and vapor-phase reactivity into models, and (3) extensive evaluation against ambient measurements of OC and NCOM across multiple seasons and geographic regions.

■ ASSOCIATED CONTENT

Supporting Information. Additional information as noted in the text. This material is available free of charge via the Internet at http://pubs.acs.org.

■ AUTHOR INFORMATION

Corresponding Author

*E-mail: Simon.Heather@epa.gov.

■ ACKNOWLEDGMENT

We acknowledge Rob Pinder, Tad Kleindienst, and Allen Robinson for helpful suggestions on the manuscript and thank Alice Gilliland, Steven Howard, Lucille Bender, Charles Chang, Ryan Cleary, and Lara Reynolds for preparing the inputs to our base CMAQ simulation. This work would not be possible without the support of Rohit Mathur, David Wong, Shawn Roselle, Wyat Appel, and numerous other members of the CMAQ modeling group at EPA. The United States Environmental Protection Agency produced the research described here. It has been subjected to Agency's administrative review and approved for publication.

■ REFERENCES

(1) Carlton, A. G.; Bhave, P. V.; Napelenok, S. L.; Edney, E. O.; Sarwar, G.; Pinder, R. W.; Pouliot, G. A.; Houyoux, M. Model representation of secondary organic aerosol in CMAQv4.7. *Environ. Sci. Technol.* **2010**, *44* (22), 8553–8560.

(2) de Gouw, J. A.; Middlebrook, A. M.; Warneke, C.; Goldan, P. D.; Kuster, W. C.; Roberts, J. M.; Fehsenfeld, F. C.; Worsnop, D. R.; Canagaratna, M. R.; Pszenny, A. A. P.; et al. Budget of organic carbon in a polluted atmosphere: Results from the New England Air Quality Study in 2002. *J. Geophys. Res.-Atmos.* **2005**, *110* (D16), D16305.

(3) Foley, K. M.; Roselle, S. J.; Appel, K. W.; Bhave, P. V.; Pleim, J. E.; Otte, T. L.; Mathur, R.; Sarwar, G.; Young, J. O.; Gilliam, R. C.; et al. Incremental testing of the Community Multiscale Air Quality (CMAQ) modeling system version 4.7. *Geosci. Model Dev.* **2010**, *3*, 205–226.

(4) Goldstein, A. H.; Galbally, I. E. Known and unexplored organic constituents in the earth's atmosphere. *Environ. Sci. Technol.* **2007**, *41* (5), 1514–1521.

(5) Hallquist, M.; Wenger, J. C.; Baltensperger, U.; Rudich, Y.; Simpson, D.; Claeys, M.; Dommen, J.; Donahue, N. M.; George, C.; Goldstein, A. H.; et al. The formation, properties and impact of secondary organic aerosol: Current and emerging issues. *Atmos. Chem. Phys.* **2009**, *9* (14), 5155–5236.

(6) Heald, C. L.; Jacob, D. J.; Park, R. J.; Russell, L. M.; Huebert, B. J.; Seinfeld, J. H.; Liao, H.; Weber, R. J. A large organic aerosol source in the free troposphere missing from current models. *Geophys. Res. Lett.* **2005**, *32* (18), L18809.

(7) Johnson, D.; Utembe, S. R.; Jenkin, M. E.; Derwent, R. G.; Hayman, G. D.; Alfarra, M. R.; Coe, H.; McFiggans, G. Simulating regional scale secondary organic aerosol formation during the TORCH 2003 campaign in the southern UK. *Atmos. Chem. Phys.* **2006**, *6*, 403–418.

(8) Simpson, D.; Yttri, K. E.; Klimont, Z.; Kupiainen, K.; Caseiro, A.; Gelencsér, A.; Pio, C.; Puxbaum, H.; Legrand, M. Modeling carbonaceous aerosol over Europe: Analysis of the CARBOSOL and EMEP EC/OC campaigns. *J. Geophys. Res.-Atmos.* **2007**, *112* (D23), D23s14.

(9) Volkamer, R.; Jimenez, J. L.; San Martini, F.; Dzepina, K.; Zhang, Q.; Salcedo, D.; Molina, L. T.; Worsnop, D. R.; Molina, M. J. Secondary organic aerosol formation from anthropogenic air pollution: Rapid and higher than expected. *Geophys. Res. Lett.* **2006**, *33* (17), L17811.

(10) Bahreini, R.; Ervens, B.; Middlebrook, A. M.; Warneke, C.; de Gouw, J. A.; DeCarlo, P. F.; Jimenez, J. L.; Brock, C. A.; Neuman, J. A.; Ryerson, T. B.; et al. Organic aerosol formation in urban and industrial plumes near Houston and Dallas, Texas. *J. Geophys. Res.-Atmos.* **2009**, *114*, D00f16.

(11) Dzepina, K.; Volkamer, R. M.; Madronich, S.; Tulet, P.; Ulbrich, I. M.; Zhang, Q.; Cappa, C. D.; Ziemann, P. J.; Jimenez, J. L. Evaluation of recently-proposed secondary organic aerosol models for a case study in Mexico City. *Atmos. Chem. Phys.* **2009**, *9* (15), 5681–5709.

(12) Farina, S. C.; Adams, P. J.; Pandis, S. N. Modeling global secondary organic aerosol formation and processing with the volatility basis set: Implications for anthropogenic secondary organic aerosol. *J. Geophys. Res.-Atmos.* **2010**, *115*, D09202.

(13) Henze, D. K.; Seinfeld, J. H.; Ng, N. L.; Kroll, J. H.; Fu, T.-M.; Jacob, D. J.; Heald, C. L. Global modeling of secondary organic aerosol formation from aromatic hydrocarbons: High- vs. low-yield pathways. *Atmos. Chem. Phys.* **2008**, *8* (9), 2405–2420.

(14) Henze, D. K.; Seinfeld, J. H. Global secondary organic aerosol from isoprene oxidation. *Geophys. Res. Lett.* **2006**, *33* (9), L09812.

(15) Sakulyanontvittaya, T.; Guenther, A.; Helmig, D.; Milford, J.; Wiedinmyer, C. Secondary organic aerosol from sesquiterpene and monoterpene emissions in the United States. *Environ. Sci. Technol.* **2008**, *42* (23), 8784–8790.

(16) Carlton, A. G.; Turpin, B. J.; Altieri, K. E.; Seitzinger, S. P.; Mathur, R.; Roselle, S. J.; Weber, R. J. CMAQ model performance enhanced when in-cloud secondary organic aerosol is included: Comparisons of organic carbon predictions with measurements. *Environ. Sci. Technol.* **2008**, *42* (23), 8798–8802.

(17) Chen, J.; Griffin, R. J.; Grini, A.; Tulet, P. Modeling secondary organic aerosol formation through cloud processing of organic compounds. *Atmos. Chem. Phys.* **2007**, *7* (20), 5343–5355.

(18) Ervens, B.; Feingold, G.; Frost, G. J.; Kreidenweis, S. M. A modeling study of aqueous production of dicarboxylic acids: 1. Chemical pathways and speciated organic mass production. *J. Geophys. Res.-Atmos.* **2004**, *109* (D15), D15205.

(19) Ervens, B.; Volkamer, R. Glyoxal processing by aerosol multiphase chemistry: Towards a kinetic modeling framework of secondary organic aerosol formation in aqueous particles. *Atmos. Chem. Phys.* **2010**, *10* (17), 8219–8244.

(20) Jimenez, J. L.; Canagaratna, M. R.; Donahue, N. M.; Prevot, A. S. H.; Zhang, Q.; Kroll, J. H.; DeCarlo, P. F.; Allan, J. D.; Coe, H.; Ng, N. L.; et al. Evolution of organic aerosols in the atmosphere. *Science* **2009**, *326* (5959), 1525–1529.

(21) Robinson, A. L.; Donahue, N. M.; Shrivastava, M. K.; Weitkamp, E. A.; Sage, A. M.; Grieshop, A. P.; Lane, T. E.; Pierce, J. R.; Pandis, S. N. Rethinking organic aerosols: Semivolatile emissions and photochemical aging. *Science* **2007**, *315* (5816), 1259–1262.

(22) Hodzic, A.; Jimenez, J. L.; Madronich, S.; Canagaratna, M. R.; DeCarlo, P. F.; Kleinman, L.; Fast, J. Modeling organic aerosols in a megacity: Potential contribution of semi-volatile and intermediate volatility primary organic compounds to secondary organic aerosol formation. *Atmos. Chem. Phys.* **2010**, *10* (12), 5491–5514.

(23) Pye, H. O. T.; Seinfeld, J. H. A global perspective on aerosol from low-volatility organic compounds. *Atmos. Chem. Phys.* **2010**, *10* (9), 4377–4401.

(24) Grieshop, A. P.; Donahue, N. M.; Robinson, A. L. Laboratory investigation of photochemical oxidation of organic aerosol from wood fires 2: Analysis of aerosol mass spectrometer data. *Atmos. Chem. Phys.* **2009**, *9* (6), 2227–2240.

(25) Murphy, B. N.; Pandis, S. N. Simulating the formation of semivolatile primary and secondary organic aerosol in a regional chemical transport model. *Environ. Sci. Technol.* **2009**, *43* (13), 4722–4728.

(26) Shrivastava, M. K.; Lane, T. E.; Donahue, N. M.; Pandis, S. N.; Robinson, A. L. Effects of gas particle partitioning and aging of primary emissions on urban and regional organic aerosol concentrations. *J. Geophys. Res.-Atmos.* **2008**, *113* (D18), D18301.

(27) Bhave, P. V.; Pouliot, G. A.; Zheng, M. Diagnostic model evaluation for carbonaceous $PM_{2.5}$ using organic markers measured in the southeastern US. *Environ. Sci. Technol.* **2007**, *41* (5), 1577–1583.

(28) Rogge, W. F.; Hildemann, L. M.; Mazurek, M. A.; Cass, G. R.; Simoneit, B. R. T. Mathematical modeling of atmospheric fine particle-associated primary organic compound concentrations. *J. Geophys. Res.-Atmos.* **1996**, *101* (D14), 19379–19394.

(29) Roy, A. A.; Wagstrom, K. M.; Adams, P. J.; Pandis, S. N.; Robinson, A. L. Quantification of the effects of molecular marker oxidation on source apportionment estimates for motor vehicles. *Atmos. Environ.* **2011**, *45* (18), 3132–3140.

(30) Hodzic, A.; Jimenez, J. L.; Madronich, S.; Aiken, A. C.; Bessagnet, B.; Curci, G.; Fast, J.; Lamarque, J. F.; Onasch, T. B.; Roux, G.; et al. Modeling organic aerosols during MILAGRO: Importance of biogenic secondary organic aerosols. *Atmos. Chem. Phys.* **2009**, *9* (18), 6949–6981.

(31) Kleindienst, T. E.; Jaoui, M.; Lewandowski, M.; Offenberg, J. H.; Lewis, C. W.; Bhave, P. V.; Edney, E. O. Estimates of the

contributions of biogenic and anthropogenic hydrocarbons to secondary organic aerosol at a southeastern US location. *Atmos. Environ.* **2007**, *41* (37), 8288–8300.

(32) Hildemann, L. M.; Klinedinst, D. B.; Klouda, G. A.; Currie, L. A.; Cass, G. R. Sources of urban contemporary carbon aerosol. *Environ. Sci. Technol.* **1994**, *28* (9), 1565–1576.

(33) Hodzic, A.; Jimenez, J. L.; Prevot, A. S. H.; Szidat, S.; Fast, J. D.; Madronich, S. Can 3-D models explain the observed fractions of fossil and non-fossil carbon in and near Mexico City? *Atmos. Chem. Phys.* **2010**, *10* (22), 10997–11016.

(34) Bhave, P. V., Yu, S., Lewis, C. W. Evaluation of a model for predicting the fossil-fuel and biogenic contributions to fine particulate carbon. American Association of Aerosol Research, 11B1, Austin, TX, October 2005.

(35) Fast, J.; Aiken, A. C.; Allan, J.; Alexander, L.; Campos, T.; Canagaratna, M. R.; Chapman, E.; DeCarlo, P. F.; de Foy, B.; Gaffney, J.; et al. Evaluating simulated primary anthropogenic and biomass burning organic aerosols during MILAGRO: Implications for assessing treatments of secondary organic aerosols. *Atmos. Chem. Phys.* **2009**, *9* (16), 6191–6215.

(36) Tsimpidi, A. P.; Karydis, V. A.; Zavala, M.; Lei, W.; Molina, L.; Ulbrich, I. M.; Jimenez, J. L.; Pandis, S. N. Evaluation of the volatility basis-set approach for the simulation of organic aerosol formation in the Mexico City metropolitan area. *Atmos. Chem. Phys.* **2010**, *10* (2), 525–546.

(37) Heald, C. L.; Kroll, J. H.; Jimenez, J. L.; Docherty, K. S.; DeCarlo, P. F.; Aiken, A. C.; Chen, Q.; Martin, S. T.; Farmer, D. K.; Artaxo, P. A simplified description of the evolution of organic aerosol composition in the atmosphere. *Geophys. Res. Lett.* **2010**, *37*, L08803.

(38) Pang, Y.; Turpin, B. J.; Gundel, L. A. On the importance of organic oxygen for understanding organic aerosol particles. *Aerosol Sci. Technol.* **2006**, *40* (2), 128–133.

(39) Chhabra, P. S.; Flagan, R. C.; Seinfeld, J. H. Elemental analysis of chamber organic aerosol using an Aerodyne high-resolution aerosol mass spectrometer. *Atmos. Chem. Phys.* **2010**, *10*, 4111–4131.

(40) Reff, A.; Bhave, P. V.; Simon, H.; Pace, T. G.; Pouliot, G. A.; Mobley, J. D.; Houyoux, M. Emissions inventory of $PM_{2.5}$ trace elements across the United States. *Environ. Sci. Technol.* **2009**, *43* (15), 5790–5796.

(41) Robinson, A. L.; Donahue, N. M.; Rogge, W. F., Photochemical oxidation and changes in molecular composition of organic aerosol in the regional context. *J. Geophys. Res.-Atmos.* **2006**, *111* (D3)

(42) Turpin, B. J.; Lim, H.-J. Species contributions to $PM_{2.5}$ mass concentrations: Revisiting common assumptions for estimating organic mass. *Aerosol Sci. Technol.* **2001**, *35* (1), 602–610.

(43) Brewer, P. F.; Adlhoch, J. P. Trends in speciated fine particulate matter and visibility across monitoring networks in the southeastern United States. *J. Air Waste Manage. Assoc.* **2005**, *55* (11), 1663–1674.

(44) Chow, J. C.; Watson, J. G.; Chen, L. W. A.; Chang, M. C. O.; Robinson, N. F.; Trimble, D.; Kohl, S. The IMPROVE-A temperature protocol for thermal/optical carbon analysis: Maintaining consistency with a long-term database. *J. Air Waste Manage. Assoc.* **2007**, *57* (9), 1014–1023.

(45) Chow, J. C.; Watson, J. G.; Crow, D.; Lowenthal, D. H.; Merrifield, T. Comparison of IMPROVE and NIOSH carbon measurements. *Aerosol Sci. Technol.* **2001**, *34* (1), 23–34.

(46) Aiken, A. C.; DeCarlo, P. F.; Kroll, J. H.; Worsnop, D. R.; Huffman, J. A.; Docherty, K. S.; Ulbrich, I. M.; Mohr, C.; Kimmel, J. R.; Sueper, D.; et al. O/C and OM/OC ratios of primary, secondary, and ambient organic aerosols with high-resolution time-of-flight aerosol mass spectrometry. *Environ. Sci. Technol.* **2008**, *42* (12), 4478–4485.

(47) DeCarlo, P. F.; Kimmel, J. R.; Trimborn, A.; Northway, M. J.; Jayne, J. T.; Aiken, A. C.; Gonin, M.; Fuhrer, K.; Horvath, T.; Docherty, K. S.; et al. Field-deployable, high-resolution, time-of-flight aerosol mass spectrometer. *Anal. Chem.* **2006**, *78* (24), 8281–8289.

(48) Chen, J. J.; Mao, H. T.; Talbot, R. W.; Griffin, R. J. Application of the CACM and MPMPO modules using the CMAQ model for the eastern United States. *J. Geophys. Res.-Atmos.* **2006**, *111* (D23), D23s25.

(49) Murphy, B. N.; Donahue, N. M.; Fountoukis, C.; Pandis, S. N. Simulating the oxygen content of ambient organic aerosol with the 2D volatility basis set. *Atmos. Chem. Phys.* **2011**, *11* (15), 7859–7873.

(50) George, I. J.; Abbatt, J. P. D. Heterogeneous oxidation of atmospheric aerosol particles by gas-phase radicals. *Nat. Chem.* **2010**, *2* (9), 713–722.

(51) George, I. J.; Slowik, J.; Abbatt, J. P. D. Chemical aging of ambient organic aerosol from heterogeneous reaction with hydroxyl radicals. *Geophys. Res. Lett.* **2008**, *35* (13), L13811.

(52) Altieri, K. E.; Seitzinger, S. P.; Carlton, A. G.; Turpin, B. J.; Klein, G. C.; Marshall, A. G. Oligomers formed through in-cloud methylglyoxal reactions: Chemical composition, properties, and mechanisms investigated by ultra-high resolution FT-ICR mass spectrometry. *Atmos. Environ.* **2008**, *42* (7), 1476–1490.

(53) Kalberer, M.; Paulsen, D.; Sax, M.; Steinbacher, M.; Dommen, J.; Prevot, A. S. H.; Fisseha, R.; Weingartner, E.; Frankevich, V.; Zenobi, R.; et al. Identification of polymers as major components of atmospheric organic aerosols. *Science* **2004**, *303* (5664), 1659–1662.

(54) Simon, H.; Bhave, P. V.; Swall, J. L.; Frank, N. H.; Malm, W. C. Determining the spatial and seasonal variability in OM/OC ratios across the US using multiple regression. *Atmos. Chem. Phys.* **2011**, *11* (6), 2933–2949.

(55) Appel, K. W.; Bhave, P. V.; Gilliland, A. B.; Sarwar, G.; Roselle, S. J. Evaluation of the community multiscale air quality (CMAQ) model version 4.5: Sensitivities impacting model performance; Part II—Particulate matter. *Atmos. Environ.* **2008**, *42* (24), 6057–6066.

(56) Weitkamp, E. A.; Lambe, A. T.; Donahue, N. M.; Robinson, A. L. Laboratory measurements of the heterogeneous oxidation of condensed-phase organic molecular makers for motor vehicle exhaust. *Environ. Sci. Technol.* **2008**, *42* (21), 7950–7956.

(57) Lambe, A. T.; Miracolo, M. A.; Hennigan, C. J.; Robinson, A. L.; Donahue, N. M. Effective rate constants and uptake coefficients for the reactions of organic molecular markers (*n*-alkanes, hopanes, and steranes) in motor oil and diesel primary organic aerosols with hydroxyl radicals. *Environ. Sci. Technol.* **2009**, *43* (23), 8794–8800.

(58) George, I. J.; Vlasenko, A.; Slowik, J. G.; Broekhuizen, K.; Abbatt, J. P. D. Heterogeneous oxidation of saturated organic aerosols by hydroxyl radicals: Uptake kinetics, condensed-phase products, and particle size change. *Atmos. Chem. Phys.* **2007**, *7* (16), 4187–4201. Model description and evaluation. *J. Geophys. Res.-Atmos.* **2001**, *106* (D19), 23073–23095.

(59) Lane, T. E.; Donahue, N. M.; Pandis, S. N. Simulating secondary organic aerosol formation using the volatility basis-set approach in a chemical transport model. *Atmos. Environ.* **2008**, *42* (32), 7439–7451.

(60) Worton, D. R.; Goldstein, A. H.; Farmer, D. K.; Docherty, K. S.; Jimenez, J. L.; Gilman, J. B.; Kuster, W. C.; de Gouw, J.; Williams, B. J.; Kreisberg, N. M.; et al. Origins and composition of fine atmospheric carbonaceous aerosol in the Sierra Nevada Mountains, California. *Atmos. Chem. Phys.* **2011**, *11* (19), 10219–10241.

(61) Chan, M. N.; Surratt, J. D.; Chan, A. W. H.; Schilling, K.; Offenberg, J. H.; Lewandowski, M.; Edney, E. O.; Kleindienst, T. E.; Jaoui, M.; Edgerton, E. S.; et al. Influence of aerosol acidity on the chemical composition of secondary organic aerosol from beta-caryophyllene. *Atmos. Chem. Phys.* **2011**, *11* (4), 1735–1751.

(62) Ng, N. L.; Canagaratna, M. R.; Jimenez, J. L.; Chhabra, P. S.; Seinfeld, J. H.; Worsnop, D. R. Changes in organic aerosol composition with aging inferred from aerosol mass spectra. *Atmos. Chem. Phys.* **2011**, *11* (13), 6465–6474.

(63) Grell, G. A.; Dudhia, J.; Stauffer, D. R. *A Description of the Fifth Generation Penn State-NCAR Mesocale Model (MM5)*; NCAR Tech. Note NCAR/TN-398+STR; National Center for Atmospheric Research: Boulder, CO, 1994; p 122.

(64) US Environmental Protection Agency technical support document: Preparation of emissions inventories for the 2002-based platform, version 3, criteria air pollutants. http://www.epa.gov/ttn/chief/emch/index.html#2002 (accessed 2009).

(65) Bey, I.; Jacob, D. J.; Yantosca, R. M.; Logan, J. A.; Field, B. D.; Fiore, A. M.; Li, Q. B.; Liu, H. G. Y.; Mickley, L. J.; Schultz, M. G. Global

modeling of tropospheric chemistry with assimilated meteorology: Model description and evaluation. *J. Geophys. Res. Atmos.* **2001**, *106*, 23073–23095.

(66) Bae, M.-S.; Demerjian, K. L.; Schwab, J. J. Seasonal estimation of organic mass to organic carbon in $PM_{2.5}$ at rural and urban locations in New York state. *Atmos. Environ.* **2006**, *40* (39), 7467–7479.

(67) DeCarlo, P. F.; Ulbrich, I. M.; Crounse, J.; de Foy, B.; Dunlea, E. J.; Aiken, A. C.; Knapp, D.; Weinheimer, A. J.; Campos, T.; Wennberg, P. O.; Jimenez, J. L. Investigation of the sources and processing of organic aerosol over the central Mexican plateau from aircraft measurements during MILAGRO. *Atmos. Chem. Phys.* **2010**, *10* (12), 5257–5280.

(68) DeCarlo, P. F.; Dunlea, E. J.; Kimmel, J. R.; Aiken, A. C.; Sueper, D.; Crounse, J.; Wennberg, P. O.; Emmons, L.; Shinozuka, Y.; Clarke, A.; et al. Fast airborne aerosol size and chemistry measurements above Mexico City and Central Mexico during the MILAGRO campaign. *Atmos. Chem. Phys.* **2008**, *8* (14), 4027–4048.

(69) Dunlea, E. J.; DeCarlo, P. F.; Aiken, A. C.; Kimmel, J. R.; Peltier, R. E.; Weber, R. J.; Tomlinson, J.; Collins, D. R.; Shinozuka, Y.; McNaughton, C. S.; et al. Evolution of Asian aerosols during transpacific transport in INTEX-B. *Atmos. Chem. Phys.* **2009**, *9* (19), 7257–7287.

(70) Sun, Y.; Zhang, Q.; Macdonald, A. M.; Hayden, K.; Li, S. M.; Liggio, J.; Liu, P. S. K.; Anlauf, K. G.; Leaitch, W. R.; Steffen, A.; et al. Size-resolved aerosol chemistry on Whistler Mountain, Canada with a high-resolution aerosol mass spectrometer during INTEX-B. *Atmos. Chem. Phys.* **2009**, *9* (9), 3095–3111.

(71) Mohr, C.; Huffman, J. A.; Cubison, M. J.; Aiken, A. C.; Docherty, K. S.; Kimmel, J. R.; Ulbrich, I. M.; Hannigan, M.; Jimenez, J. L. Characterization of primary organic aerosol emissions from meat cooking, trash burning, and motor vehicles with high-resolution aerosol mass spectrometry and comparison with ambient and chamber observations. *Environ. Sci. Technol.* **2009**, *43* (7), 2443–2449.

(72) Huffman, J. A.; Docherty, K. S.; Mohr, C.; Cubison, M. J.; Ulbrich, I. M.; Ziemann, P. J.; Onasch, T. B.; Jimenez, J. L. Chemically-resolved volatility measurements of organic aerosol from different sources. *Environ. Sci. Technol.* **2009**, *43* (14), 5351–5357.

(73) Malm, W. C.; Hand, J. L. An examination of the physical and optical properties of aerosols collected in the IMPROVE program. *Atmos. Environ.* **2007**, *41* (16), 3407–3427.

(74) El-Zanan, H. S.; Lowenthal, D. H.; Zielinska, B.; Chow, J. C.; Kumar, N. Determination of the organic aerosol mass to organic carbon ratio in IMPROVE samples. *Chemosphere* **2005**, *60* (4), 485–496.